HETEROCYCLES, Vol. 104, No. 5, 2022, pp. 878 - 893. © 2022 The Japan Institute of Heterocyclic Chemistry
Received, 15th November, 2021, Accepted, 31st January, 2022, Published online, 9th February, 2022
DOI: 10.3987/COM-21-14590

THEORETICAL INVESTIGATION ON THE MECHANISM AND SELECTIVITY OF CATALYST-FREE ANNULATION OF YNEDIONES AND (ISO)QUINOLINE *N*-OXIDES

Nan Lu,* Hui Liang, Chengxia Miao, and Xiaozheng Lan

The affiliations are desired to be typewritten in English. College of Chemistry and Material Science, Shandong Agricultural University, Taian City 271018, Shandong Prov., P.R. China; E-mail: lun@sdau.edu.cn

Abstract – The mechanism is investigated for tandem annulation of ynedione and (iso)quinoline *N*-oxide without catalyst using M06-2X functional. The [3 + 2] cycloaddition generates active isoxazolo[3,2-*a*]isoquinoline in stage 1, which undergoes ring-opening delivering tautomerization intermediates. A series of imine-enamine and keto-enol tautomerism takes place in stage 2. Four competitive paths exist in stage 3. The pure N-nucleophilic addition and one concerted path involving asynchronous hydrogen transfer generate pyrrolo[2,1-*a*]isoquinoline and pyrrolo[1,2-*a*]quinoline. The by-product (isoquinolin-1-yl)-2,5-diphenylfuran is difficult to obtain owing to the unavailability of starting intermediate of O-nucleophilic addition. The high regioselectivity is controlled both by thermodynamics and kinetics in stage 3. The energy barriers of most steps are decreased in THF solution verifying an advantageous solvation effect. The competitive N- and O-nucleophilic additions are supported by Multiwfn analysis on Frontier Molecular Orbital and Mayer bond order of vital transition states.

INTRODUCTION

As structural core of marine natural alkaloids,[1] pyrrolo[2,1-*a*]isoquinoline has a wide spectrum of pharmacological activities[2] and potential attractive properties in biological activities.[3] The crucial issue for the construction of this scaffold has gained considerable attention and prompts the development of a large number of synthetic methods. In terms of catalyst selection, transition metals are commonly used such as nickel-catalyzed cyclization strategy for the synthesis of pyrroloquinolines, tandem palladium-catalyzed intermolecular allylic alkylation/allylic dearomatization reaction, gold-catalyzed

atom-economic synthesis of sulfone-containing pyrrolo[2,1-*a*]isoquinoline starting from pyrroles, quinolines, and diynamides, respectively.[4-6] A series of acid and base catalysts have been reported initiated by various isoquinolines. The intermolecular cyclization of substituted 3-aryl (heteroaryl)-3-chloroacrylaldehydes can be promoted by trimethylamine in one pot.[7] The $PhCO_2H$-mediated intermolecular [3 + 2] cycloaddition provides a concise total synthesis of lamellarin core from (*E*)-(2-nitrovinyl)benzenes and azomethine ylides.[8] The pyrrolo[2,1-*a*]isoquinolines and coumarin-fused pentacyclic derivatives have been constructed by DMAP-dependent annulation of 4-chloro-3-formylcoumarin.[9] There's also a recent boost in research involving chemoselective synthesis of polycyclic isoquinolinones, tandem quinolone-alkyne-cyclization and oxidative [3 + 2] cycloaddition promoted by diethyl azodicarboxylate.[10-12]

The reactivity of conjugated α,β-ynone and α-diketone is remarkable in synthetic organic chemistry,[13,14] especially the annulation of ynedione possessing alkynyl and continuous two-carbonyl groups.[15] Görgen has reported an efficient synthesis of 1,5-diacyl-5-hydroxypyrazolines in a consecutive three-component fashion via one-pot activation−alkynylation−cyclization reaction of (hetero)arylglyoxylic acids, oxalyl chloride, arylacetylenes, and hydrazides.[16] Nagaraju has achieved regioselectivity-switchable annulations between alkynyl α-diketones and α-cyanoketones catalyzed by Brønsted base for the first time, delivering a series of dihydrofurofuran and furan derivatives. The work demonstrates unique features of alkynyl α-diketone in sharp contrast to that of ynone-related chemistry.[17] Chen has obtained hydroxy spirocyclopenteneindenedione with strong crystallization-induced emission and data storage application via cascade annulation between alkynyl 1,2-diketones and indene-1,3-diones.[18] However, these reactions usually need catalyst or additive or high temperature.

From green and sustainable perspective, it is desirable to prepare pyrrolo[2,1-*a*]isoquinolines under catalyst- and additive-free conditions. In this field, the recent experimental work has constructed 3-((iso)-quinolin-1-yl)-4*H*-chromen-4-ones, 13*H*-isoquinolino[2,1-*a*]quinolin-13-ones and 3-(2-quinolyl)-chromones from ynones and *N*-oxides via solvent-controlled annulation[19] and transition-metal-free tandem reaction,[20] separately. In the progress of efficient way, of special interest to us is Wang's group, who has synthesized pyrrolo[2,1-*a*]isoquinolines and pyrrolo[1,2-*a*]quinolines from ynediones and (iso)quinoline *N*-oxides.[21] To the best of our knowledge, in addition to some successful transition of ynones, there is no report about mechanistic study for the cyclization of ynediones.[19,22] Although a tandem [3 + 2] cycloaddition/ring-opening/N-nucleophilic addition is proposed, the simple description is not sufficient to provide detailed mechanism especially the origin of regioselectivity. Is there any difference or similarity between the real mechanism and the above generally accepted one? Since the by-product exists with a certain yield in the competition between O- and N-nucleophilic additions, why the former is inferior to the latter? As an indication of substrate scope, is the reaction process of quinoline

N-oxide consistent with that of isoquinoline *N*-oxide? To solve these experimental and mechanistic problems, an in-depth theoretical study[23] was performed to draw a detailed picture of the new simple and efficient annulation of ynediones and (iso)quinoline *N*-oxides. The density functional theory (DFT) method was applied also focusing on the enantioselectivity not mentioned in experiment at all.[24,25]

RESULTS AND DISCUSSION

Based on the experimental studies reported previously,[21] the detailed mechanism has been explored for tandem annulation of 1,4-diphenylbut-3-yne-1,2-dione **1a** and isoquinoline *N*-oxide **2a** leading to pyrrolo[2,1-*a*]isoquinoline **3aa** and (isoquinolin-1-yl)-2,5-diphenylfuran **4aa** (Scheme 1). As depicted in Scheme 2, the reaction includes three stages: (1) the [3 + 2] cycloaddition of **1a** with **2a** generates active isoxazolo[3,2-*a*]isoquinoline **I**, which undergoes ring-opening delivering tautomerization intermediates **II**, (2) the imine-enamine and keto-enol tautomerism among five isomers denoted as **IIa**, **IIb**, **IIc**, **IId**, and **IIe**, (3) different concerted N- and O-nucleophilic additions starting from various **II**. The energies for all stationary points are calculated relative to the sum of isolated substrates (Supplementary Table S1). Since the reaction occurs in THF solvent in experiment, the Gibbs free energies in solution phase are mainly discussed.

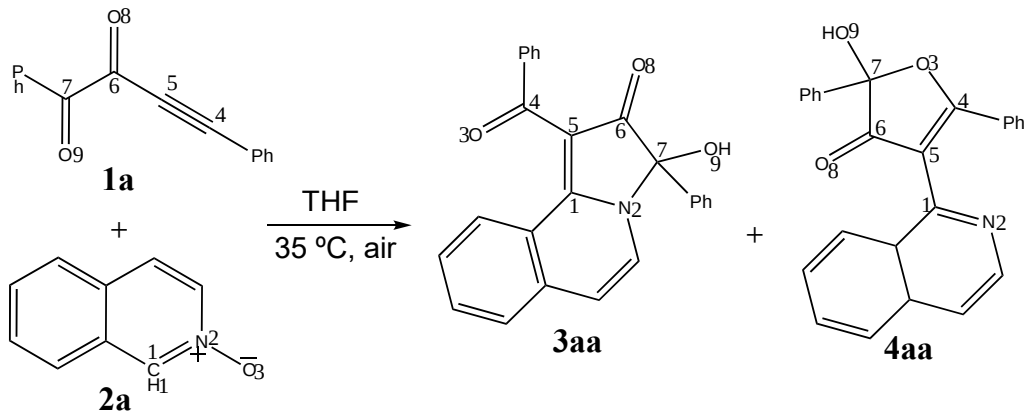

Scheme 1. Tandem annulation of 1,4-diphenylbut-3-yne-1,2-dione **1a** and isoquinoline *N*-oxide **2a** leading to pyrrolo[2,1-*a*]isoquinoline **3aa** and (isoquinolin-1-yl)-2,5-diphenylfuran **4aa**.

[3 + 2] Cycloaddition and ring-opening

The stage 1 includes [3 + 2]cycloaddition and ring-opening marked with green solid arrow in Scheme 2. Two steps are located as is described by the relative Gibbs free energy profile and optimized structure of TSs (Figure 1). The initial complex **im1** is stable with energy of -7.58 kcal mol^{-1} relative to reactants **1a** and **2a**. Step1 of [3 + 2]cycloaddition occurs via transition state **ts-ca** (-299 cm^{-1}) with a free energy barrier of 16.96 kcal mol^{-1} (Table 1) with respect to **im1**

forming stable intermediate **I** exergonic by -37.32 kcal mol^{-1}. "**ca**" represents cycloaddition. The transition vector corresponds to an array of vibration modes indicating a concerted cyclization. The detailed description of atomic motion during this course includes remarkable shortening of C1···C5 and O3···C4 distances (2.37, 1.84 Å) (Supplementary Figure S1a). Comparatively, the stretching of C1-N2, N2-O3 and C4–C5 bonds (1.34, 1.31, 1.26 Å) are not very obvious as an assistant role. Once C1-C5 and O3-C4 are completely bonded, a five membered ring is formed in the resulted isoxazolo[3,2-*a*]isoquinoline **I** (Scheme 2, Supplementary Figure S2).

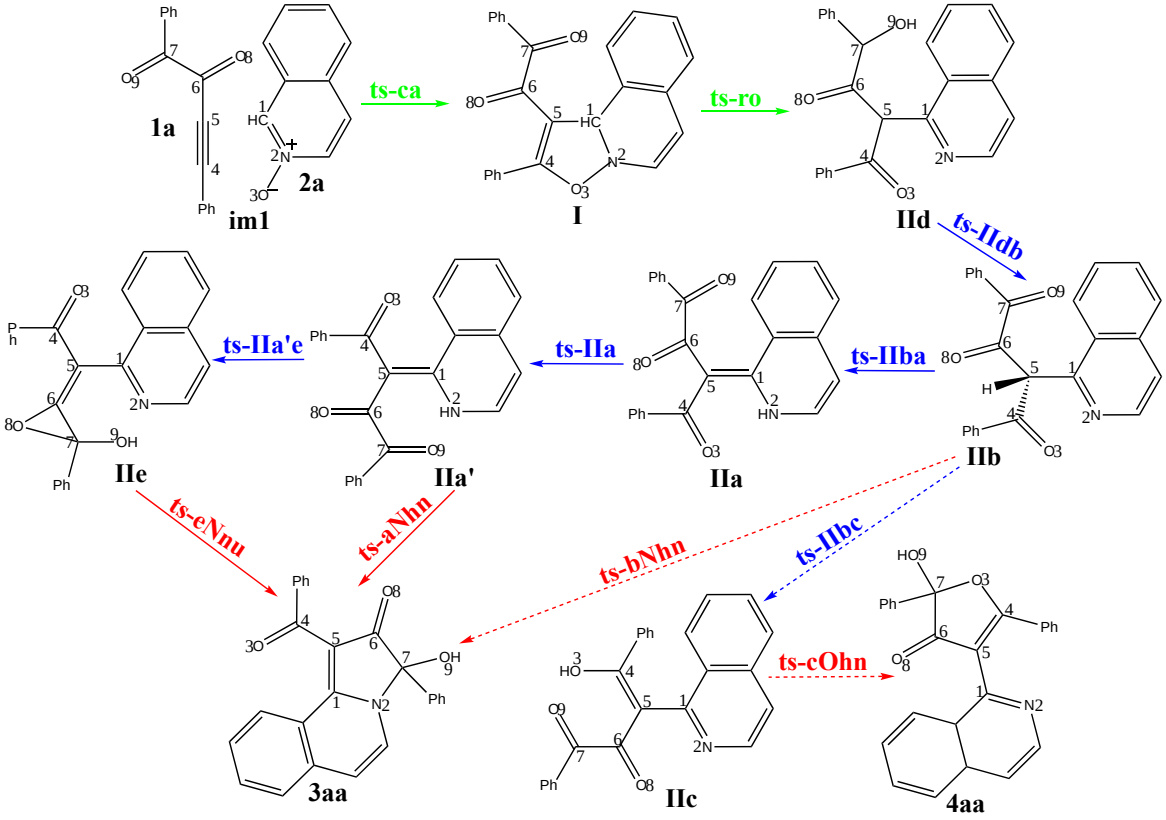

Scheme 2. Proposed mechanism of tandem annulation of **1a** with **2a**. The initial complex between **1a** and **2a** is denoted as **im1**. [3 + 2] cycloaddition and ring-opening are marked with green solid arrow (stage 1) giving isoxazolo[3,2-*a*]isoquinoline **I** and intermediate **II**. The tautomerization among a series of **II** (**a**, **b**, **c**, **d**, **e**) is marked with blue solid arrow (stage 2). N-nucleophilic addition is marked with red solid arrow (stage 3) leading to product **3aa**. The unfavorable processes in each stage are marked with dotted arrow using the same color.

In step2, the ring-opening of **I** proceeds via **ts-ro** (-151 cm^{-1}) with a free energy barrier decreased to 8.25 kcal mol^{-1} (Table 1). "**ro**" represents ring-opening. This step is enormously exergonic by -63.78 kcal mol^{-1} leading to intermediate **IId** as a typical imine-enol structure with C1-N2 double bond and O9-H1 bond (Scheme 2, Supplementary Figure S2). Although **IId** is not mentioned by Wang,[21] the correctness can be approved by the vibration modes illustrated in Figure S1b. Essentially, the transition vector of **ts-ro** contains conspicuous departure of H1 from C1 to O9

(1.11, 2.20 Å) and cleavage of N2–O3 bond (2.28 Å). In a synchronous manner, the C4-C5 double bond stretches to single one together with the contraction of C1-N2 and C4–O3 single bonds to double (1.43, 1.43, 1.25 Å). Owing to the continuous heat release of two steps, stage 1 is quite favourable for the initiation of next stage from thermodynamics perspective. Compared with relatively easy ring-opening, the [3 + 2]cycloaddition is determined to be rate-limiting in stage 1 kinetically. **IId** is selected as starting point of stage 2 to investigate various tautomerization marked with blue arrows (Scheme 2).

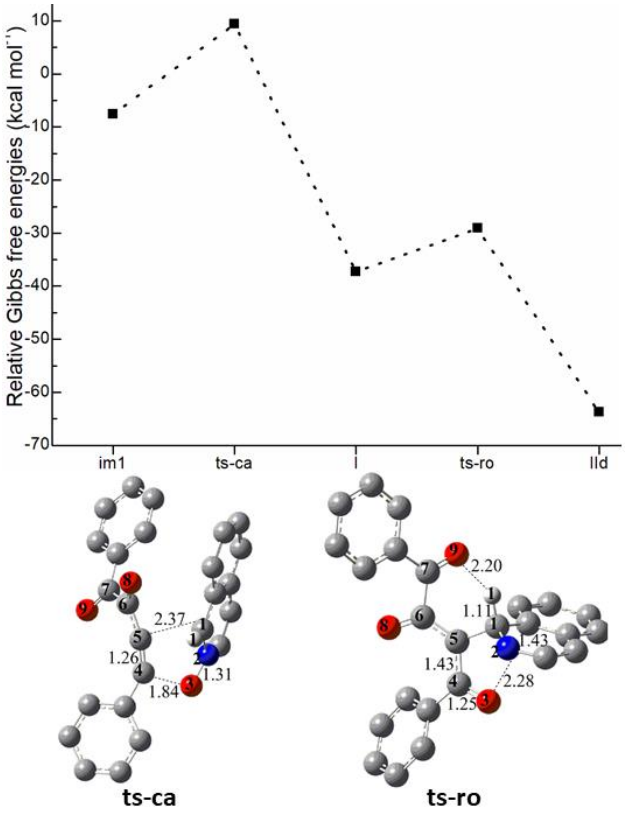

Figure 1. Relative Gibbs free energy profile in solvent phase for [3 + 2] cycloaddition and ring-opening starting from **im1** calculated with M06-2X/6-311++G(d,p)//M06-2X/6-31G(d). Bond lengths in optimized structure of transition states are given in angstroms. Hydrogen atoms on methyl and benzene ring are removed for clarity.

Table 1. The Gibbs free energy barrier (in kcal mol^{-1}) of all reactions in the gas and solution phase calculated with M06-2X/6-311++G(d,p)//M06-2X/6-31G(d) method

TS	$\Delta G^{\neq}_{gas}$	$\Delta G^{\neq}_{sol}$	TS	$\Delta G^{\neq}_{gas}$	$\Delta G^{\neq}_{sol}$
ts-ca	15.64	16.96	**ts-eca**	16.20	14.89
ts-ro	20.53	8.25	**ts-ero**	22.62	12.43

ts-IIdb	2.77	9.91	**ts-eIIdb**	-11.77	-3.12
ts-IIba	39.49	35.10	**ts-eIIba**	43.12	35.21
ts-IIbc	49.12	50.82	**ts-eIIa**	16.97	5.59
ts-IIa	13.72	7.80	**ts-eIIa'e**	25.49	27.55
ts-IIa'e	23.27	24.62			
ts-eNnu	7.18	5.22	**ts-eeNnu**	7.90	3.82
ts-aNhn	35.79	31.66	**ts-eaNhn**	27.59	21.25
ts-bNhn	41.53	44.19	**ts-ebNhn**	33.12	38.19
ts-cOhn	21.13	14.10			

Imine-enamine and keto-enol tautomerism

For stage 2 of tautomerism among a series of **II** (**a**, **b**, **c**, **d**, **e**), the feasible paths are described by the relative Gibbs free energy profile and optimized structure of TSs (Figure 2). In this stage, TS is named according to the two intermediates it connects. Shown by the black dotted line, the main process is denoted as path A comprising four steps starting from complex **IId**. The step1 takes place via transition state **ts-IIdb** (-792 cm^{-1}) with a small barrier of 9.91 kcal mol^{-1} (Table 1) exergonic by -91.20 kcal mol^{-1} generating **IIb**, in which C5-H1 bond is formed after the transfer of H1 from O9 to C5 (1.12, 1.65 Å). In step2, H1 shifts from C5 to N2 (1.51, 1.31 Å) via transition state **ts-IIba** (1782i) with an increased barrier of 35.10 kcal mol^{-1} yielding N2-H1 bond in **IIa**. The imine isomerizes to enamine, making the energy of **IIa** only 0.49 kcal mol^{-1} higher than that of **IIb**. The two benzene rings of **1a** flip in step3 via transition state **ts-IIa** (59i), which is characterized by a dihedral angle of C4-C5-C6-C1 (-167°). Through **ts-IIa**, atom H1 close to O3 in the structure of **IIa** turns to be approaching O9 in its isomer **IIa'** (Scheme 2, Supplementary Figure S2). The energy of **IIa'** is 5.71 kcal mol^{-1} uphill from that of **IIa** due to the weakened π-π stacking effect. Despite this, the energy barrier is low to be 7.80 kcal mol^{-1} favourably from kinetics. Another more active intermediate **IIe** was also located in step4 with energy 22.2 kcal mol^{-1} higher than that of **IIa'**. Via transition state **ts-IIa'e** (-266 cm^{-1}), the barrier is increased to be 24.62 kcal mol^{-1} with respect to **IIa'**. The transition vector of **ts-IIa'e** contains concerted moving of H1 from N2 to O9 (1.64, 1.04 Å) and approaching of O8 to C7 (1.86 Å). This not only

produces O9-H1 bond representing enol structure but a ternary ring with large tension in resultant **IIe**, which also involves imine recovered from enamine.

From **IIb**, an alternative path B seems to be available as presented by the blue dotted arrow in Scheme 2 and blue dotted line in Figure 2. Via transition state **ts-IIbc** (-1857 cm^{-1}), C5 gives H1 to O3 (1.50, 1.25 Å) generating O3-H1 bond in enol structure **IIc**. However, the energy barrier of path B is increased to be 50.82 kcal mol^{-1} indicating the disadvantage kinetically. Such energy barrier was too large to overcome under ambient temperature in original experimental conditions. Furthermore, the energy of **IIc** is higher by 3.83 kcal mol^{-1} than that of enamine **IIa** also unfavourable thermodynamically. Obviously, step2 of path A is rate-limiting in stage 2. Although the barrier is somewhat high, the rate constant *k* is calculated to be about $3.3*10^{-9}$ s^{-1} applying the experimental temperature (35 °C). When the free energy barrier is used to investigate the reality of a reaction, it is affected by the model simplification, accuracy of method and basis set, as well as the mathematical treatment. The error can reach several kcal mol^{-1}. So the value with M06-2X/6-311++G(d,p) only could roughly indicates that step2 is difficult to occur yet not completely impossible.

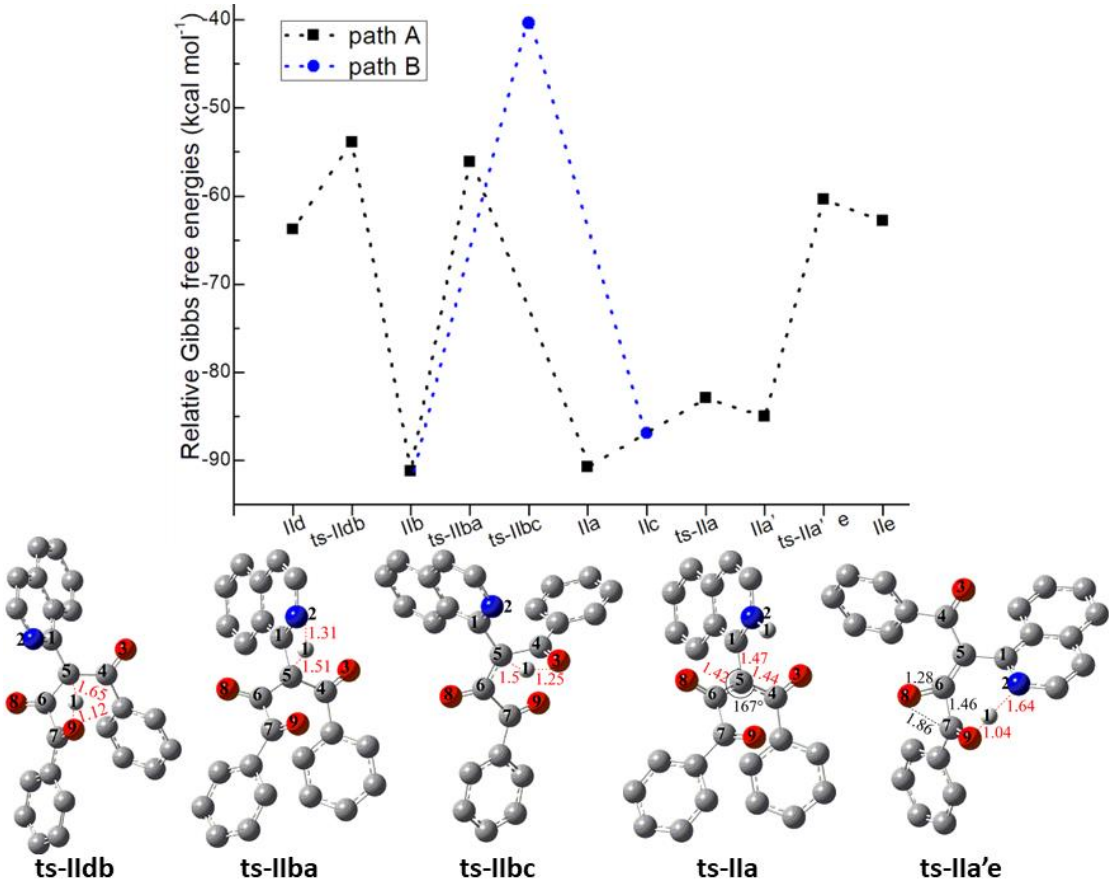

Figure 2. Relative Gibbs free energy profile in solvent phase for tautomerization among a series of **II** (**a**, **b**, **c**, **d**, **e**) starting from complex **IId** calculated with M06-2X/6-311++G(d,p)//M06-2X/6-31G(d). Bond lengths in optimized structure of transition states are given in angstroms. Hydrogen atoms on methyl and benzene ring are removed for clarity.

N- and O-nucleophilic addition

In stage 3, four possible concerted paths are located according to the nucleophilic pattern and illustrated by the relative Gibbs free energy profile of Figure 3 together with the optimized structure of TSs. "eNnu, aNhn, bNhn, cOhn" were used to distinguish N-nucleophilic, hydrogen transfer/N-nucleophilic and hydrogen transfer/O-nucleophilic paths starting from complexes **IIe**, **IIa'**, **IIb**, **IIc**, respectively. Among the four possible initial intermediates, the most reactive is **IIe**, from which the pure N-nucleophilic addition occurs via **ts-eNnu** (-122 cm^{-1}) with the lowest free energy barrier of 5.22 kcal mol^{-1} (Table 1). Due to the ternary ring existing in **IIe**, the transition vector contains a ring opening and the synchronous nucleophilic process described in detail by the atomic motion during this course (Supplementary Figure S1c). That is the conspicuous breaking of C7-O8, forming of N2-C7 (2.11, 2.53 Å) and the cooperating elongation of C6-C7, shortening of C6–O8 bonds (1.50, 1.25 Å). Based on N2-C7 bond, the annulation is accomplished affording a five membered ring in the desired product **3aa** exergonic by -101.31 kcal mol^{-1} (Scheme 2, Supplementary Figure S2). Both of the other two paths yielding **3aa** consist of hydrogen transfer followed by N-nucleophilic addition in concerted mode from **IIb** and **IIa**, respectively. As is depicted by Figure S1d, when H1 transfers from C5 to O9 (1.65, 1.12 Å) via **ts-bNhn** (-810 cm^{-1}), a slight delay of the N2-C7 bonding (2.63 Å) indicates an asynchronous process. However, the high energy barrier with respect to **IIb** (44.19 kcal mol^{-1}) suggests that bNhn path is unrealistic under ambient temperature in experimental conditions. Alternatively, via **ts-aNhn** (-130 cm^{-1}), the barrier is reduced to be 31.66 kcal mol^{-1} initiating from **IIa'**. Figure S1e provides detailed atomic motion comprising H1 moving from enamine N2 to O9 (1.95, 1.11 Å) and the asynchronous bonding of N2-C7 (2.86 Å). Thereby, for the major N-nucleophilic process, eNnu path is superior to aNhn whether from the energy barrier or from the exergonic energy.

As by-product, **4aa** was obtained by a concerted asynchronous hydrogen transfer and O-nucleophilic addition path denoted as cOhn competitive with other three. Exhibited by the red dotted line of Figure 3 from **IIc**, this course proceeds via **ts-cOhn** (-127 cm^{-1}) with an energy barrier of 14.10 kcal mol^{-1} and exergonic by -97.05 kcal mol^{-1} giving **4aa** (Scheme 2, Supplementary Figure S2). The transition vector corresponds to the H1 leaving from enol O3 to O9 (2.21, 1.10 Å) and the bonding of O3-C7 (2.47 Å) (Figure S1f). Although cOhn path seems to be feasible in stage 3, the starting **IIc** is impossible to form from **IIb** verified above. Thus **4aa** could not be obtained from **IIc**, which is inconsistent to the experiment result by Wang.[21]

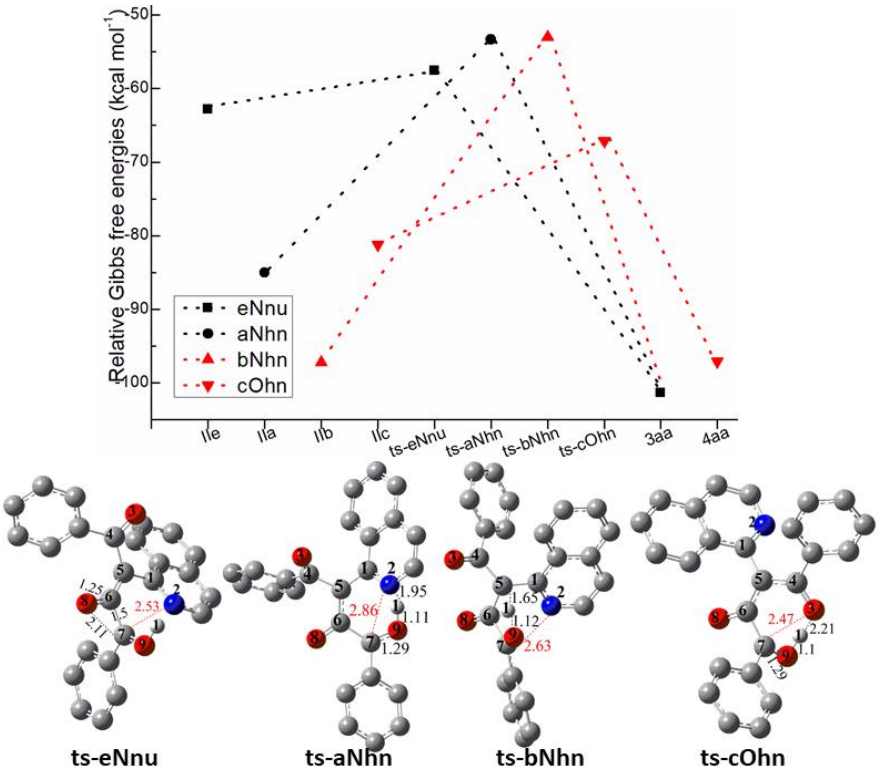

Figure 3. Relative Gibbs free energy profile in solvent phase for N- and O-nucleophilic additions starting from complexes **IIe**, **IIa**, **IIb**, **IIc** calculated with M06-2X/6-311++G(d,p)//M06-2X/6-31G(d). Bond lengths in optimized structure of transition states are given in angstroms. Hydrogen atoms on methyl and benzene ring are removed for clarity.

Regioselectivity and substrate tolerance

The regioselectivity of a reaction is indicated quantitatively by the ratio of main and by-product. Here the yield (%) **3aa**/**4aa** in THF solvent was 90/4 reported by experiment.[21] Based on the above mechanism analysis, the origin of high regioselectivity is presumed to lie in eNnu and cOhn two competitive paths of N- and O-nucleophilic addition in stage 3. On one hand, from kinetics perspective, the barrier of eNnu path is 8.88 kcal mol^{-1} lower in energy than that of cOhn path. It's thus clear that the formation of N2-C7 bond is much easier to achieve than that of O3-C7 bond. On the other, the relative energy of **3aa** is 4.26 kcal mol^{-1} lower by than that of **4aa**. Evidently, in terms of product stability, the aza five membered ring is more stable than oxa one denoting the preference of **3aa** as main product thermodynamically. It can be seen that the regioselectivity is simultaneously controlled by thermodynamics and kinetics. Quantitatively, the yield **3aa**/**4aa** could be predicted by employing exothermic or barrier differences between competitive paths.[26-30] The ratio is calculated to be far greater than 99/1 using a difference of 4.26 or 8.88 kcal mol^{-1}. This just reflects the existence rationality of another bNhn and aNhn paths. Compared with pure N-nucleophilic eNnu, both two paths possess higher barrier whereas less

exothermic energy. Inevitably, this will lower the advantage of main product to some extent reducing the ratio (>>99/1) to close to 90/4 in accordance with experiment.

The tandem annulation of quinoline *N*-oxide **2e** with **1a** was also explored to investigate the substrate tolerance. The O-nucleophilic addition and **IIc** related to by-product are not considered in the comparison between main product pyrrolo[1,2-*a*]quinoline **3ae** and the above pyrrolo[2,1-*a*]isoquinoline **3aa**. Seen from the optimized structures of TSs given by Figure 4, the overall reaction process is completely consistent. So the difference of energy barrier is mainly discussed. Compared with the reaction of **1a** with **2a**, in stage 1, the barrier of [3 + 2] cycloaddition via **ts-eca** (-93 cm^{-1}) is decreased to 14.89 kcal mol^{-1} while that of ring-opening via **ts-ero** (-135 cm^{-1}) is increased to 12.43 kcal mol^{-1} narrowing the difference between two steps. The discrepancy of stage 2 is about H1 transfer from O9 to C5 and flipping of two benzene rings. For the reaction involving **2e**, the process of step1 and step3 becomes quite readily accessible via **ts-eIIdb** (-1110 cm^{-1}) and **ts-eIIba** (-1763 cm^{-1}) with greatly reduced barriers (-3.12 and 5.59 kcal mol^{-1}). The relative energy of **ts-eIIdb** is even lower than that of **eIId** resulting in a value less than zero. In stage 3, three paths are all easier via **ts-eeNnu** (-343 cm^{-1}), **ts-ebNhn** (-1438 cm^{-1}), **ts-eaNhn** (-131 cm^{-1}) leading to **3ae** than the case of **3aa** owing to the different degrees of barrier reduction (-1.40, -6.00, -10.41 kcal mol^{-1}). Thermodynamically, **3ae** is 3.14 kcal mol^{-1} more stable than **3aa** with energy of -104.45 kcal mol^{-1} in solution phase. Apparently, **3ae** can also be obtained by the tandem annulation with **2e** as reactant. This not only agrees with experiment, but explains the high yield of pyrrolo[1,2-*a*]quinoline.[21]

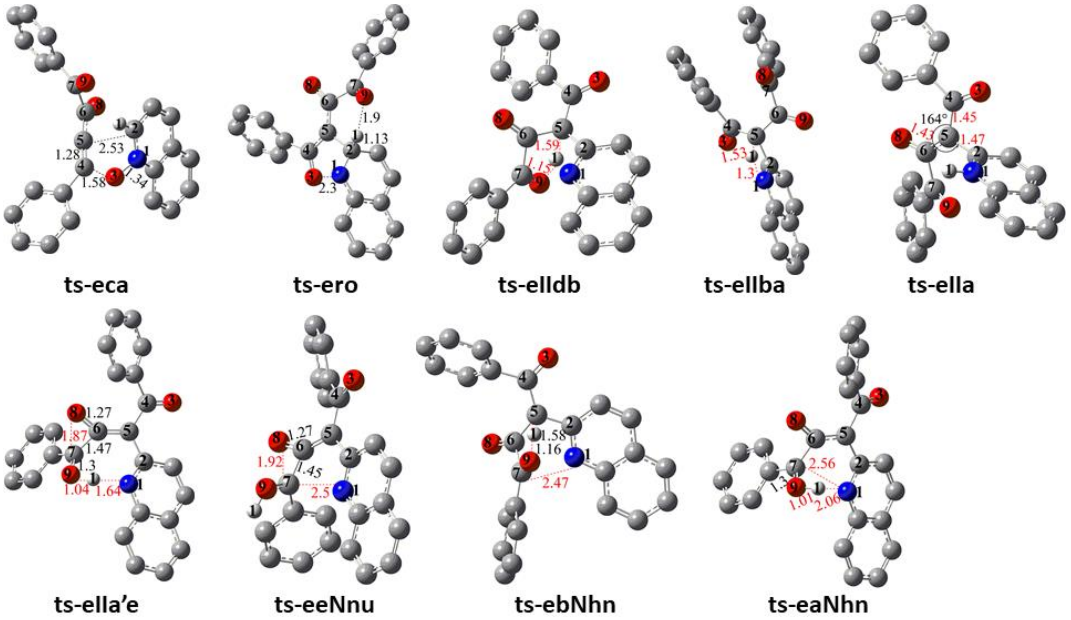

Figure 4. Optimized structure of transition states for the tandem annulation of quinoline *N*-oxide **2e** with **1a** calculated with M06-2X/6-311++G(d,p)//M06-2X/6-31G(d). Bond lengths are given in angstroms. Hydrogen atoms on methyl and benzene ring are removed for clarity.

Solvent effect and FMO analysis

In view of the great solvent effect on reaction involving ions estimated by our approach,[26-29] it's expected to have little impact on this uncharged system. The difference values between in gas phase and THF solution are listed with regard to relative energy and energy barrier for all stationary points (Supplementary Table S1 and Table S2). Entirely, the relative energies of intermediate are slightly increased. But the added value does not exceed 5 kcal mol^{-1}. For most transition states, the relative energies are decreased. In contrast, the reduction extent is relatively large while still lower than 10 kcal mol^{-1}. Generally, the energy barrier in solution should be lower than that in gas phase, which is the normal effect of solvent from kinetics. The larger the reduction value, the more favourable the path. Here fortunately, the barriers of steps in large majority are downhill with the decreased degree of -5~-13 kcal mol^{-1}. For very few steps, the ascending range of energy barrier is lower than 5 kcal mol^{-1}. Accordingly, the influence of solvation on main process of tandem annulation of ynedione with (iso)quinoline *N*-oxide is moderately advantageous from a kinetic point of view.

FMO calculations were performed to get more qualitative evidence of the structural analysis, better description of electron distribution and bonding characteristics in complex. The contribution from orbitals of bonding atoms and MBO values were calculated using Multiwfn_3.7_dev (Table 2 and Table 3)[28,29] as well as the visual orbitals of Highest Occupied Molecular Orbital (HOMO) and Lowest Unoccupied Molecular Orbital (LUMO) (Figure 5). The typical **ts-eNnu**, **ts-bNhn**, **ts-aNhn** and **ts-cOhn** are selected to analyse four competitive paths of N- and O-nucleophilic additions. The delocalization of electron density is beneficial for the stability of structure.[26-30] For **ts-eNnu**, **ts-bNhn** and **ts-aNhn**, although the MBO values of N2···C7 are lower than 0.1 in common, the electron density of HOMO on N2 is about 6%~9% together with 33%~39% of LUMO on C7 allowing for the nucleophilic attack of N2 to C7. There's little difference of the main distribution on other atoms between **ts-eNnu** and **ts-aNhn**. However, MBO values of C7···O8 (0.40) and C6···O8 (1.22) in **ts-eNnu** supports the stretching character of O8 from C6 and C7. The obvious hydrogen transfer feature of **ts-aNhn** can be demonstrated by MBO values of N2···H1 (0.21) and H1···O9 (0.54). For **ts-bNhn**, the contributions of C5 (27.07%), H1 (2.06%) on HOMO and of O9 (13.45%) on LUMO make it ready for H1 shifting from C5 to O9. This is further revealed by MBO values of C5···H1 (0.32) and H1···O9 (0.44). HOMO density of **ts-cOhn** distributed on O3 (6.01%), LUMO on C7 (36.65%) and O9 (9.01%) facilitates concerted hydrogen transfer and O-nucleophilic addition.

Table 2. Contribution (%) of Natural Atomic Orbital (NAO) to Highest Occupied Molecular Orbital (HOMO) and Lowest Unoccupied Molecular Orbital (LUMO) of typical transition states calculated with M06-2X/6-311++G(d,p)//M06-2X/6-31G(d) method (>2)

	N2	C7	C6	O8	H1	C5	O9	O3
ts-eNnu HOMO	6.36		5.04	15.52				
ts-eNnu LUMO		33.85		6.77			7.98	
ts-bNhn HOMO	8.39			6.65	2.06	27.07	3.94	
ts-bNhn LUMO		33.58		3.78			13.45	
ts-aNhn HOMO	7.08		4.31	20.50				
ts-aNhn LUMO		38.49		4.34			10.65	
ts-cOhn HOMO			4.37	12.00				6.01
ts-cOhn LUMO		36.65		6.49			9.01	

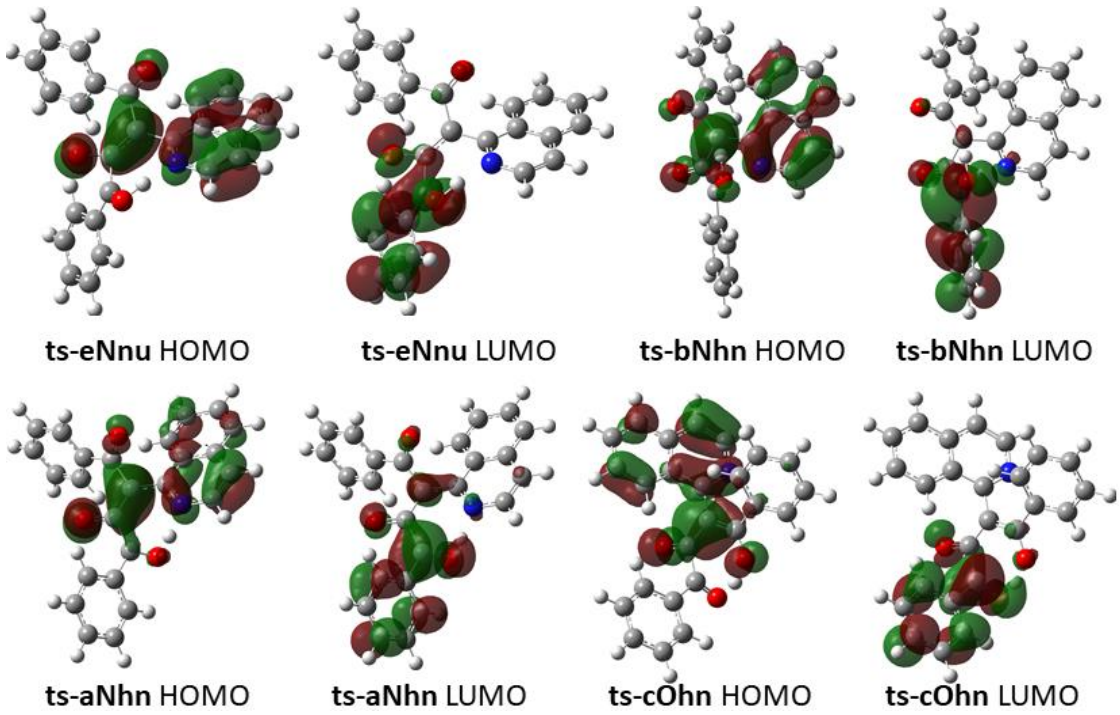

Figure 5. Highest Occupied Molecular Orbital (HOMO) and Lowest Unoccupied Molecular Orbital (LUMO) of typical transition states **ts-eNnu**, **ts-bNhn**, **ts-aNhn**, **ts-cOhn**. Different colors are used to identify the phase of the wave functions.

Table 3. Mayer bond order (MBO) of typical transition states corresponding to N- and O-nucleophilic additions calculated with M06-2X/6-311++G(d,p)//M06-2X/6-31G(d) method (>0.1)

	C6⋯C7	O3⋯C7	C7⋯O8	C6⋯O8	C5⋯H1	N2⋯H1	O3⋯H1	H1⋯O9
ts-eNnu	0.95		0.40	1.22				0.63
ts-bNhn	0.86			1.82	0.32			0.44
ts-aNhn	0.91			1.53		0.21		0.54
ts-cOhn	0.90	0.10		1.50				0.70

CONCLUSIONS

Our DFT calculations provide the first theoretical investigation on tandem annulation of ynedione and (iso)quinoline *N*-oxide without catalyst. The whole process comprises three stages. In stage 1, the [3 + 2] cycloaddition generates active species isoxazolo[3,2-*a*]isoquinoline, which undergoes ring-opening delivering tautomerization intermediates. A series of possible imine-enamine and keto-enol tautomerism takes place in stage 2. There are four competitive paths in stage 3. The most favourable is pure N-nucleophilic addition leading to pyrrolo[2,1-*a*]isoquinoline and pyrrolo[1,2-*a*]quinoline as main products, which can also be obtained via concerted path involving asynchronous hydrogen transfer. The by-product (isoquinolin-1-yl)-2,5-diphenylfuran is difficult to obtain owing to the unavailability of starting intermediate of O-nucleophilic addition. The origin of high regioselectivity is determined to be controlled both by thermodynamics and kinetics in stage 3.

Compared with those in gas phase, the relative energies of intermediates are slightly increased in THF solution while of TSs decreased as well as the energy barriers of most steps. This verifies an advantageous solvation effect on main process from a kinetic point of view. The competitiveness of N- and O-nucleophilic addition is further supported by Multiwfn analysis on FMO of typical TSs. Alternative path is also confirmed by MBO value of vital bonding and contribution of atomic orbital.

EXPERIMENTAL

Optimized structures were obtained at M06-2X/6-31G(d) level of theory with GAUSSIAN 09.[31] In tests of popular DFT methods,[32] M06-2X functional attained smaller standard deviation of difference between calculated value and experimental value in geometries than B3LYP and LSDA. The best compromise between accuracy and time consumption was provided with 6-31G(d) basis set on energy calculations.[33] Also, M06-2X functional was found to give relatively accurate results for catalysed enantioselective [4 +

3], concerted [4 + 2], stepwise [2 + 2] cycloaddition and catalysed Diels−Alder reactions.[14,34] Together with the best performance on noncovalent interaction, M06-2X functional is believed to be suitable for this system.[25] Frequencies were analysed at the same level to characterize the nature of stationary points (energy minima or first-order saddle-points) and to provide free energies at 298.15 K and 1 atm pressure, which include entropic contributions by considering the vibrations, rotations, and translations of the structures. When necessary, the intrinsic reaction coordinate (IRC) calculations were performed to verify the right connections among a transition state (TS) and its forward, backward minima.

To consider the solvent effect on the reaction, single-point calculations with self-consistent reaction field[35-37] were applied for all gas-phase optimized structures at M06-2X/6-311++G(d,p) level based on the integral equation formalism polarizable continuum model (IEFPCM)[38] with united-atom Kohn-Sham (UAKS) radii and cavity-dispersion-solvent-structure terms in Truhlar and co-workers' "density" solvation model[39] for tetrahydrofuran (THF). For all cited energies, zero point energy (ZPE) corrections were taken into account. The frontier molecular orbital (FMO) calculations were performed in order to characterize the changes in electronic properties and bonding orbital interaction. The FMO theory coupled with density functional calculation provides an efficient method for comparing different reaction pathways. In FMO theory, the energies, atomic orbital coefficients, net atomic charges and orbital overlaps of FMOs can be used to estimate relative chemical reactivity.[40-42] Furthermore, we used the Multiwfn_3.7_dev package[43] to perform wave function analysis such as Mayer bond order (MBO), the composition of FMO, orbital delocalization index (DI), and electron localization function (ELF)-π plots.

SUPPORTING INFORMATION

Supplementary data available: [Computation information and cartesian coordinates of stationary points; Calculated relative energies for the ZPE-corrected Gibbs free energies (ΔGgas), and Gibbs free energies (ΔGsol) for all species in solution phase at 298 K; Optimized structures of selected intermediates and transition states.] Supplementary data (Experimental procedures and details, Characterization data for products, NMR spectra for all compounds) associated with this article can be found, in the onlineversion, at URL: https://www.heterocycles.jp/newlibrary/downloads/PDFsi/27502/104/5.

ACKNOWLEDGEMENTS

This work was supported by National Natural Science Foundation of China (21973056, 21972079) and Natural Science Foundation of Shandong Province (ZR2019MB050).

REFERENCES AND NOTES

1. H. Fan, J. Peng, M. T. Hamann, and J.-F. Hu, *Chem. Rev.*, 2008, **108**, 264.
2. C. Bailly, *Mar. Drugs*, 2015, **13**, 1105.
3. A. Hazra, S. Mondal, A. Maity, S. Naskar, P. Saha, R. Paira, K. B. Sahu, P. Paira, S. Ghosh, C. Sinha, A. Samanta, S. Banerjee, and N. B. Mondal, *Eur. J. Med. Chem.*, 2011, **46**, 2132.
4. S. Thavaselvan and K. Parthasarathy, *Org. Lett.*, 2020, **22**, 3810.
5. H.-J. Zhang, Z.-P. Yang, Q. Gu, and S.-L. You, *Org. Lett.*, 2019, **21**, 3314.
6. J. Liu, P. Chakraborty, H. Zhang, L. Zhong, Z.-X. Wang, and X. Huang, *ACS Catal.*, 2019, **9**, 2610.
7. Z. Yang, N. Lu, Z. Wei, J. Cao, D. Liang, H. Duan, and Y. Lin, *J. Org. Chem.*, 2016, **81**, 11950.
8. K.-L. Zheng, M.-Q. You, W.-M. Shu, Y.-D. Wu, and A.-X. Wu, *Org. Lett.*, 2017, **19**, 2262.
9. S. Vyasamudri and D.-Y. Yang, *J. Org. Chem.*, 2019, **84**, 3662.
10. Z.-Q. Wang, C. Hou, Y.-F. Zhong, Y.-X. Lu, Z.-Y. Mo, Y.-M. Pan, and H.-T. Tang, *Org. Lett.*, 2019, **21**, 9841.
11. D. Szamosvári, K. Sylvester, P. Schmid, K.-Y. Lu, E. R. Derbyshire, and T. Böttcher, *Chem. Commun.*, 2019, **55**, 7009.
12. Y.-W. Xu, J. Wang, G. Wang, and L. Zhen, *J. Org. Chem.*, 2021, **86**, 91.
13. C. Nájera, L. K. Sydnes, and M. Yus, *Chem. Rev.*, 2019, **119**, 11110.
14. X. Li, X. Kong, S. Yang, M. Meng, X. Zhan, M. Zeng, and X. Fang, *Org. Lett.*, 2019, **21**, 1979.
15. R. E. Whittaker and G. Dong, *Org. Lett.*, 2015, **17**, 5504.
16. C. Görgen, K. Boden, G. J. Reiss, W. Frank, and T. J. J. Müller, *Beilstein J. Org. Chem.*, 2019, **15**, 1360.
17. S. Nagaraju, S. Liu, J. Liu, S. Yang, R. Liu, Z. Chen, B. Paplal, and X. Fang, *Org. Lett.*, 2019, **21**, 10075.
18. Z. Chen, F. Yu, R. Liu, X. Lin, S. Yang, J. Liu, B. Chen, S. Nagaraju, M. Zeng, C. Ding, and X. Fang, *Org. Lett.*, 2020, **22**, 2381.
19. W.-W. Yang, L.-L. Chen, P. Chen, Y.-F. Ye, Y.-B. Wang, and X. Zhang, *Chem. Commun.*, 2020, **56**, 1183.
20. J. Liu, D. Ba, Y. Chen, S. Wen, and G. Cheng, *Chem. Commun.*, 2020, **56**, 4078.
21. W.-W. Yang, Y.-F. Ye, L.-L. Chen, J.-Y. Fu, J.-Y. Zhu, and Y.-B. Wang, *J. Org. Chem.*, 2021, **86**, 169.
22. L.-L. Chen, J.-W. Zhang, P. Chen, S. Zhang, W.-W. Yang, J.-Y. Fu, J.-Y. Zhu, and Y.-B. Wang, *Org. Lett.*, 2019, **21**, 5457.
23. K. N. Houk and P. H. Y. Cheong, *Nature*, 2008, **455**, 309.
24. N. Lu, L. Meng, D. Z. Chen, and G. Q. Zhang, *J. Mol. Catal. A: Chem.*, 2011, **339**, 99.

25. N. Lu, L. Meng, D. Z. Chen, and G. Q. Zhang, *J. Phys. Chem. A*, 2012, **116**, 670.
26. N. Lu and H. T. Wang, *Dalton Trans.*, 2013, **42**, 13931.
27. N. Lu, Y. X. Bu, and H. T. Wang, *Phys. Chem. Chem. Phys.*, 2016, **18**, 2913.
28. N. Lu, X. Lan, C. Miao, and P. Qian, *Int. J. Quantum Chem.*, 2020, **120**, e26340. https://doi.org/10.1002/qua.26340.
29. N. Lu, H. Liang, P. Qian, X. Lan, and C. Miao, *Int. J. Quantum Chem.*, 2020, **120**, e26574. https://doi.org/10.1002/qua.26574.
30. G. Frenking and N. Fröhlich, *Chem. Rev.*, 2000, **100**, 717.
31. M. J. Frisch, G. W. Trucks, H. B. Schlegel, G. E. Scuseria, M. A. Robb, J. R. Cheeseman, G. Scalmani, V. Barone, B. Mennucci, G. A. Petersson, H. Nakatsuji, M. Caricato, X. Li, H. P. Hratchian, A. F. Izmaylov, J. Bloino, G. Zheng, J. L. Sonnenberg, M. Hada, M. Ehara, K. Toyota, R. Fukuda, J. Hasegawa, M. Ishida, T. Nakajima, Y. Honda, O. Kitao, H. Nakai, T. Vreven, J. A. Montgomery Jr., J. E. Peralta, F. Ogliaro, M. Bearpark, J. J. Heyd, E. Brothers, K. N. Kudin, V. N. Staroverov, R. Kobayashi, J. Normand, K. Raghavachari, A. Rendell, J. C. Burant, S. S. Iyengar, J. Tomasi, M. Cossi, N. Rega, J. M. Millam, M. Klene, J. E. Knox, J. B. Cross, V. Bakken, C. Adamo, J. Jaramillo, R. Gomperts, R. E. Stratmann, O. Yazyev, A. J. Austin, R. Cammi, C. Pomelli, J. W. Ochterski, R. L. Martin, K. Morokuma, V. G. Zakrzewski, G. A. Voth, P. Salvador, J. J. Dannenberg, S. Dapprich, A. D. Daniels, Ö. Farkas, J. B. Foresman, J. V. Ortiz, J. Cioslowski and D. J. Fox, *Gaussian 09 Revision B.01*, Gaussian, Inc, Wallingford, CT 2009.
32. D. S. Huh and S. J. Choe, *J. Porphyrins Phthalocyanines*, 2010, **14**, 592.
33. M. Rooman and R. Wintjens, *J. Biomol. Struct. Dyn.*, 2014, **32**, 532.
34. E. H. Krenske, K. N. Houk, and M. Harmata, *J. Org. Chem.*, 2015, **80**, 744.
35. O. Tapia, *J. Math. Chem.*, 1992, **10**, 139.
36. J. Tomasi and M. Persico, *Chem. Rev.*, 1994, **94**, 2027.
37. B. Y. Simkin and I. Sheikhet, Quantum Chemical and Statistical Theory of Solutions—A Computational Approach, Ellis Horwood, London, 1995.
38. J. Tomasi, B. Mennucci, and R. Cammi, *Chem. Rev.*, 2005, **105**, 2999.
39. A. V. Marenich, C. J. Cramer, and D. G. Truhlar, *J. Phys. Chem. B*, 2009, **113**, 6378.
40. G. Klopman, *J. Am. Chem. Soc.*, 1968, **90**, 223.
41. L. Salem, *J. Am. Chem. Soc.*, 1968, **90**, 543.
42. L. Salem, *J. Am. Chem. Soc.*, 1968, **90**, 553.
43. T. Lu and F. Chen, *J. Comput. Chem.*, 2012, **33**, 580.